scientific reports

Check for updates

OPEN

A single computational model to simulate the three foot-rocker mechanisms of the gait cycle

Nicolás Yanguma-Muñoz[1], Javier Bayod[2] & Christian Cifuentes-De la Portilla[1✉]

The use of computational models of the human foot based on finite element analysis offers a promising alternative for understanding the biomechanical internal changes of this structure. However, the evaluation of dynamic scenarios has been challenging. This research aims to design a computational model that accurately simulates foot biomechanics during the stance period of the gait cycle in healthy and flatfoot scenarios. The model is focused on analyzing stress variations in soft tissues such as the plantar fascia and spring ligament to provide valuable insights into the internal biomechanics of the foot. The results were evaluated using maximum principal stress. Validation was performed by measuring clinical angles and comparing the range of motion of foot joints with known values for each phase. Results show that the plantar fascia and spring ligament stress increase during the second and third rockers compared to the first rocker. Additionally, as was expected, flatfoot simulations show stress increments in those evaluated soft tissues, while surgical treatment scenarios contributed to stress reduction in these regions. These findings emphasize the active role of the plantar fascia and spring ligament, particularly during approximately 50% of the stance period when the plantar arch deformity is greater. Results show valuable insights into the internal biomechanics of the foot through computational models.

Keywords Biomechanics, Finite elements model, Foot, Gait, Soft tissues

The foot plays an important role in providing support and absorbing impact during movement, serving as the starting point for walking[1,2]. The study of the biomechanics of this limb over the last three decades has been guided mainly by cadaveric models, pressure or force platforms, and computational models. Cadaveric models are usually the preferred option for studying the foot in clinical scenarios. However, conducting multiple experiments is not possible since the tissue tends to deteriorate after completing a test, and usually, huge costs are related to this strategy. Platforms facilitate the measurement of external kinetic variations of the foot[3–8]. Nevertheless, the study of how stress vary in ligaments and tendons has not been possible. A currently accepted strategy in the clinical environment to quantify and analyze stress behavior in foot internal tissue is the use of computational models based on finite element analysis (FEA). This tool allows the modeling of body structures and the estimation of forces, stresses, and deformations, which is very useful for complex geometries such as the human foot[9].

Foot and ankle computational models are designed based on reconstructions from medical images such as CT scans or MRIs[9]. During the simulation process, the mechanical properties used to represent the behavior of foot structures have varied over the years with technological advances and mathematical formulations. There are two types of materials reported in most articles: linear-elastic materials for simulating bones and non-linear or hyper-elastic materials assigned to cartilage and tendons.

To date, 2D and 3D models[10–18] have been developed to study foot biomechanics. However, this method has variations that can affect the results obtained during gait representation. These relevant changes include simplifications of the geometry, such as the merging of the phalanges of the foot and the lack of trabecular bone. Moreover, the type of elements used to represent cartilage, ligaments, or tendons lets the mechanical behavior of the foot be represented. Still, it does not provide a reliable evaluation of the stress changes in these structures. Additionally, in some models, the linear-elastic mechanical properties assigned to the mentioned tissues are not appropriate according to the literature.

Furthermore, due to the complexity of the foot structure, computational models typically represent only a single stance phase of gait (specifically mid-stance or second rocker) or simulate the phases of the stance

[1]Biomedical Engineering Department, Universidad de los Andes, Bogotá D.C, Colombia. [2]Aragón Institute of Engineering Research (I3A), Universidad de Zaragoza, Zaragoza, Spain. ✉email: cc.cifuentes@uniandes.edu.co

period as independent static scenarios. However, the foot is a dynamic structure, and it is necessary to propose continuous simulations to analyze the biomechanic stress in soft tissues.

In addition, the load applied to the tendons in some models is unclear concerning the boundary conditions. The authors only mentioned that the assigned load was obtained from electromyography studies reported in the literature[10–18]. However, they did not specify the percentage of this load relative to the body weight of the patients studied. Tendon load varies according to multiple physiological parameters such as muscle length, cross-sectional area, and length of muscle fibers. For this reason, the load between computational model tendons may be different. The lack of information on the force approximation from electromyography studies makes it difficult to replicate the work of active foot stabilizers in more computational models.

Additionally, one of the main limitations shared by some models representing human gait is the type of elements used to model the soft tissues. Bar elements do not allow the analysis of stress variations that may occur. Specifically, studying and understanding these changes in soft tissues is crucial, as the internal biomechanics are not detailed. Understanding the mechanical behavior of a significant portion of foot soft tissues allows for a better comprehension of their function during the gait cycle.

Finally, orthopedic specialists are increasingly using computational models to study and analyze forces, stress, and angle modifications in surgical procedures or diseases such as ankle arthroplasty, talar replacement, diabetic foot, flatfoot, and surgical planning[19–24]. These computational approaches are valuable for surgeons interested in foot biomechanics, as they can enhance and plan surgical procedures using in-silico models, thereby avoiding potential harmful effects on patients, predicting possible outcomes, and making decisions beyond their orthopedic experience. Moreover, there is a growing trend among orthopedic device companies to incorporate FEA in developing and testing their products. The medical use of computational models is crucial for their advancement and application in real-world scenarios. According to all the previous reasons related to the lack of tissue modeling and biomechanics applications, the primary aim of this study was to develop a finite element model capable of simulating foot biomechanics during the transition from initial contact to the pre-swing phases of a gait cycle (GC) and to analyze stress variations in the key passive soft tissues that support the foot arch. To achieve this goal, we created a model incorporating relevant soft tissues and specific boundary conditions, and we validated the resulting kinematics against clinical data and foot joint angles. Additionally, we investigated the maximum principal stresses ($Smax$) within the Plantar fascia and Spring ligament under flatfoot conditions and in surgical scenarios, including single and triple arthrodesis.

Materials and methods

The designed model is based on the foot model proposed by Cifuentes-De la Portilla, C. and collaborators[24]. The reconstruction was performed with computed tomography and anatomic guides. The model reconstructs a healthy human unloaded foot of a 49-year-old male with a weight of 73.3 kg, a height of 1.70 m, and a foot size of 23 cm. The model includes 26-foot bones, 24 differentiated into cortical and trabecular components. The remaining two bones are considered to have only a cortical component. Additionally, the model includes cartilages, plantar fascia (PF), spring ligament (SL), long plantar ligament (LPL), short plantar ligament (SPL), medial talocalcaneal ligament, deep transverse metatarsal ligament, Achilles tendon (AT), peroneus brevis tendon (PB) and tibialis posterior tendon (TP) (See Fig. 1). We ensure that cartilage tissues separate the joints and the TP includes the insertion of the navicular and first cuneiform[25,26].
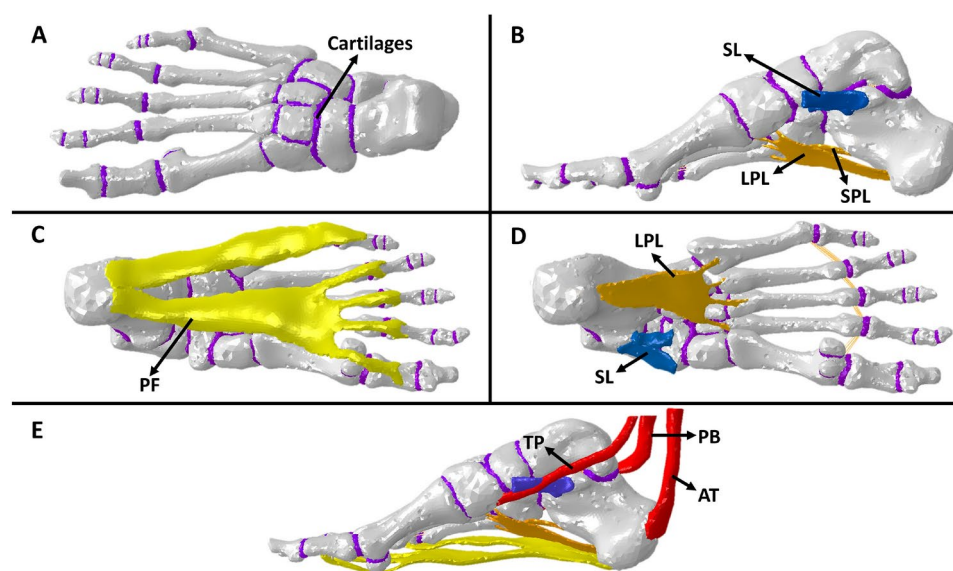

Fig. 1. Computational model, (**A**) Top view Bones and cartilages, (**B**) Sagittal view of ligaments in the model, (**C**) Bottom view of fascia plantar, (**D**) Bottom view of ligaments, (**E**) Sagittal view of all structures represented in the foot model.

Tissue	Mesh size (mm)	Element type
Cortical bone	5	Tetrahedral
Trabecular bone	4	Tetrahedral
Plantar fascia	1.5	Tetrahedral
Spring ligament	1.5	Tetrahedral
Tibialis posterior tendon	2	Tetrahedral
Peroneus brevis tendon	2	Tetrahedral
Achilles tendon	2	Tetrahedral
Short plantar ligament	2	Tetrahedral
Long plantar ligament	2	Tetrahedral
Cartilages	1–2	Tetrahedral
Talocalcaneal and metatarsal ligament		Bar element

Table 1. Mesh size and element type for segments of the finite element model.

Quality metric	Assessment criteria	Accurate elements (%)	Inaccurate elements (%)
Element jacobian	> 0.2	99.8	0.02
Aspect ratio	> 0.3	99.5	0.05

Table 2. Mesh quality metrics if computational model.

Meshing

The meshing process was performed using the software Ansys V.21 (Pennsylvania, United States, https://www.ansys.com/). A previous trial-and-error approach was employed to optimize the mesh size of each tissue in the model[13]. The following conditions were considered to achieve a reasonable mesh size without compromising the calculation time. The mesh size and type of elements of structures of the foot model are shown in Table 1. Also, to avoid large differences in element size between regions, a mesh accuracy of more than 99% of the elements being better than 0.2 mesh quality (Jacobians), and checking that the poor elements were located away from the region of greatest interest (PF, SL, and TP geometries)[27]. The meshing process was conducted using a single mesh without including any additional interactions between the foot bones.

The model has a total of 770630 linear tetrahedral elements (C3D4). All parameters were within good mesh quality ratios (See Table 2). Simulations were done in Abaqus/CAE V.6.14-1 with the non-linear solver.

Tissue modeling

Except for the cartilage and tendons, tissues were considered elastic-linear material. Based on the literature[28–30] we use the following mechanical properties: Cortical bone ($E = 17000$ MPa, $v = 0.3$), trabecular bone ($E = 700$ MPa, $v = 0.30$), ligaments ($E = 700$ MPa, $v = 0.28$) and plantar fascia ($E = 250$MPa, $v = 0.28$), E represent Young's modulus and v mean poison ratio. A non-linear and hyperelastic Ogden model was used to model both the cartilage tissue and tendons. The main reason for using the hyperelastic model was that some studies have demonstrated that cartilage displaces water under compression, thus it is better represented by the Ogden model[31,32]. Tendons are also structures in which hyperelastic models better represent mechanical behavior[16]. Its strain energy density function (U) is presented in the following equation:

$$U = \frac{\mu}{\alpha^2}(\lambda_1^\alpha + \lambda_2^\alpha + \lambda_3^\alpha - 3) + \frac{1}{D}(J - 1)^2 \tag{1}$$

where μ is the initial shear modulus, α is the strain-hardening exponent and D is the compressibility parameter. The parameters used for the cartilages are $\mu = 13.2$, $\alpha = 6.0$ y D = 0.48, and for tendons $\mu = 33.16$, $\alpha = 24.89$ y D = 0.00012[33].

Load and boundary conditions

The following load and boundary conditions were employed in the computational model during the continuous simulation of the gait stance period of a healthy patient. We assumed that the force at the beginning and the end of the stance phase was equal[34,35]. In addition, the loading conditions and constraint nodes were modified at the end of each simulation step. This means that once the simulation step corresponding to a certain phase of the stance period was completed, they were adjusted and updated to the necessary conditions for the next phase in the subsequent simulation step. In summary, the entire simulation process in ABAQUS/CAE V.6.14-1 consists of four simulation steps. The first step applies the loads and boundary conditions related to the heel-strike (first rocker) loading response. In the second step, the loads and boundary conditions are changed to those associated with the second rocker. The third step removes the previous load conditions and establishes new boundary

conditions for the third rocker. Finally, the fourth step maintains the boundary conditions from step three and applies new loads for this last simulation step.

First rocker (0–10% GC)
Corresponds to heel strike and loading response. It occurs between the first 10% of the gait cycle. The first rocker was simulated using an 864 N load representing 1.2 times body weight (BW). The load was oriented in a descending vertical direction distributed in the region of contact Tibia - Talus (80%) and Fibula - Talus (20%)[36]. The load used for the TP tendon was 21.6 N (3.0% of BW)[37,38]. The fixed nodes were in the calcaneus region blocking the movement in X, Y, and Z. The above description can be seen in the Fig. 2A,B.

Second rocker (10–50% GC)
This period corresponds to the mid-stance phase. It occurs in the 10% to 50% of the GC. The second rocker was simulated by applying a 720 N load representing the full weight of an adult person of about 73.3 kg[39], leaning on one foot. The foot load was oriented in a falling vertical direction distributed in the region of contact Tibia - Talus (90%) and Fibula - Talus (10%)[40]. The load used for the AT, TP tendon, and PB tendon were 226.8 N (31.5% of BW), 45.4 N (6.3% of BW), and 57.6 N (8.0% of BW) respectively, according to a cadaveric literature study[39]. The fixed nodes were in four regions. The first region was the calcaneus blocking the movement in X, Y, and Z. The second, third, and fourth regions block the displacements in the axis-Z and they were the head of metatarsal bones, sesamoids, and distal phalanges. The above description can be seen in the Fig. 2C,D.

Third rocker (50–60% GC)
This corresponds to the pre-swing phase. It occurs approximately between 50% and 60% of the gait cycle. The last rocker was simulated using a 2306 N load representing 3.20 times BW. The load was oriented in descending vertical direction distributed in the region of contact Tibia - Talus (90%) and Fibula - Talus (10%)[36,41]. The load used for the AT, TP tendon, and PB tendon were 2181 N (3.03 times BW), 10.8 N (2.0% of BW), and 64.8 N (10.0% of BW) respectively, according to the EMG literature values[37,38,42]. The simulation was performed with restriction nodes that fixed the movement in all axes in the proximal phalanges and axis-Z in the distal phalanges. The above description can be seen in the Fig. 2E,F.

Flatfoot and surgical scenarios simulation

In addition to simulating a healthy foot, we modeled three distinct flatfoot scenarios considering cases related to tissue damage: one with the PF reduced to 10% of its mechanical properties (Young modulus), one with the SL reduced to 10% of its mechanical properties (Young modulus), and a combined scenario with both the PF and SL reduced to 10% of their mechanical properties (Young modulus)[43,44]. These reductions were chosen because flatfoot disease is associated with the loss of biomechanical properties in the most important passive stabilizers of the plantar arch[13,29,33]. The percentage decrease corresponds to the changes observed in the slope of a strain-stress ligament curve. We consider healthy the young modulus in the linear region and pathological the young
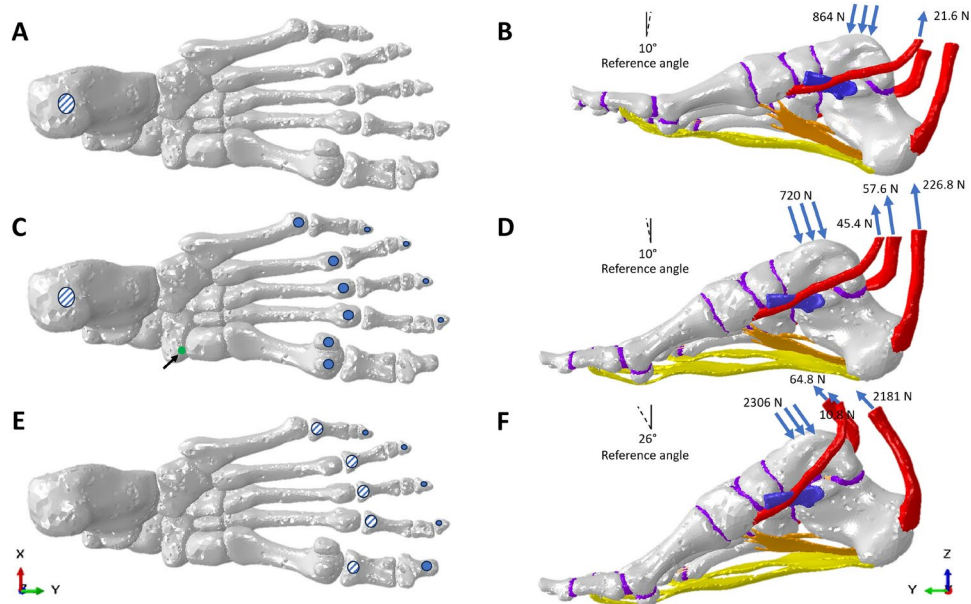

Fig. 2. Regions marked with solid circles indicate restrictions in z-displacements, while blue circles with stripes denote restrictions in x, y, and z displacements. The green circle represents the lowest point in the talus-navicular joint (**C**). This figure also illustrates the load of the tibia and fibula on the talus, the tendons included in the model, and the reference angles for the loading conditions: (**A,B**) First rocker, (**C,D**) Second rocker, and (**E,F**) Third rocker.

modules measured in the yield point[44]. Furthermore, we simulated two surgical procedures: partial subtalar and triple arthrodesis. In these surgical scenarios, the mechanical properties of the cartilage were modified to simulate cortical bone[21], representing the bone integration that occurs during arthrodesis, which effectively results in complete joint fusion (Fig. 3). The same reduced mechanical properties from the flatfoot simulations were applied to the surgical conditions, as it is assumed that the foot remains pathological, with the surgeries aiming to improve its condition. The mesh and boundary conditions used in all flatfoot and surgical simulations were consistent with those described in the previous section.

Model analysis and evaluation criteria

The variable used to evaluate the stress in soft tissues was the maximum principal stress (*SMax*). These eigenvalues are closely related to the tensile stress that is generated in foot tissues and stress refers to the maximum tensile stress during the simulation process. During the second and third rocker, the PF and SL elongate due to the support of the foot in the ground. For this reason, the main forces that support the soft tissues are related to traction forces, and the most adequate variable for measuring these changes in Abaqus/CAE V.6.14-1 is *Smax*.

Foot model validation and kinematic comparison

The base model used for these simulations was previously validated by a comparison of anatomical reference variation in two cases, loaded and unloaded[13]. However, in this case, we included more comparisons of the foot deformation by measuring two anatomical angles during mid-stance in healthy and flatfoot conditions: The internal Moreau-Costa-Bartani (IMCB) and talus-calcaneus divergence (kite's angle)[45]. Moreover, according to the range of motion of foot joints reported in kinematic studies using 3D Motion Capture system[37,46,47], this study considered three measured angles in healthy conditions: dorsiflexion/plantar flexion of the metatarsophalangeal joint, and eversion/inversion of the foot. The angles were measured using Kinovea and compared with the literature values. The IMCB angle was measured considering three anatomical landmarks. These include the most inferior point of the talus-navicular joint (Fig. 2C), the head of the first metatarsal, and the lateral malleolus. The most inferior point of the talus-navicular joint was identified as the node closer to the talus protuberance and the cartilage between the talus and the navicular bones. On the other hand, to measure the Kite angle, the projections of the medial axis of the calcaneus and the talus were considered.

Computational requirements

This study was performed using computers with the following specifications: an Intel Core i7-6700T processor, featuring 4 cores and 8 threads, and 16 GB of RAM. The simulation of the complete stance period took close to 28–29 h for all the considering simulations and utilized 94% of the available RAM.

Ethical approval

This project has the approval of the ethics committee of the engineering school of the Universidad de Los Andes. All research methods were performed following current regulations. The CT images used to design the foot model came from a volunteer who signed an informed consent form to allow the use of the images for our group's projects related to foot modeling.

Results

About model validation

Results show that the foot model generates a deformation expected in a healthy patient (IMCB: 125.1°- kite's angle: 16.9°) and flatfoot condition during the second rocker (IMCB: 133.2°- kite's angle: 26.5°)[45], as can be seen in Fig. 4.

The dorsiflexion and plantarflexion of the metatarsophalangeal joint, reported at the beginning and end of GC in the healthy condition (Fig. 5), are within the values mentioned in kinematic studies. However, this value
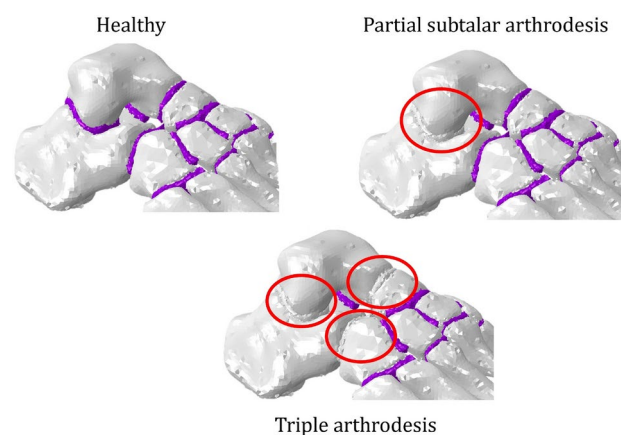

Fig. 3. Clarification of how the arthrodesis was simulated. The cartilage material was changed to a cortical bone in each fused joint.
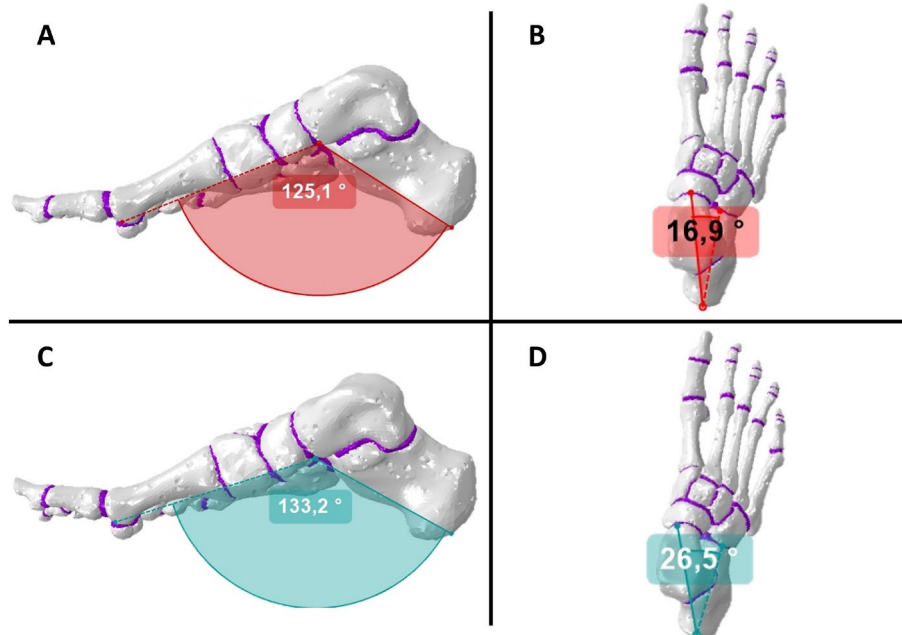
Fig. 4. Clinical angles of reference during the second rocker. The first row is the healthy condition and the second row is flatfoot disease, (**A**–**C**) IMCB angle, (**B**–**D**) Talus Calcaneus divergence (kite's angle).
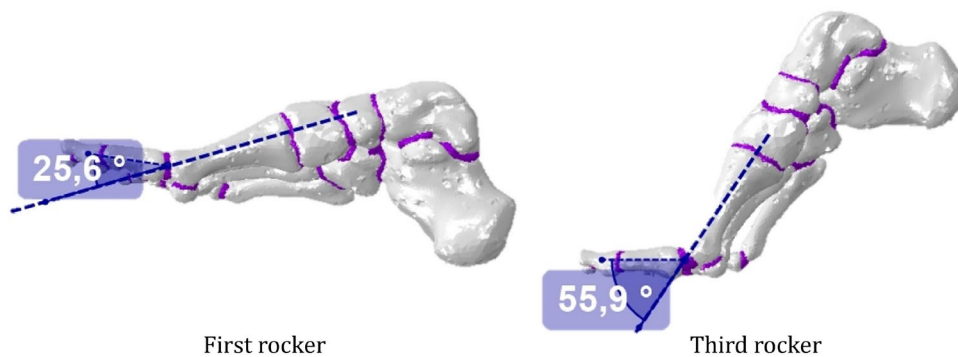

First rocker   Third rocker

Fig. 5. Dorsiflexion and plantarflexion of the metatarsophalangeal joint measured at the beginning and end of the gait cycle.

Rockers	Angle of motion reported in the literature	Angle reported by the model
First rocker	20°–30°	25.6°
Second rocker	0°–5°	8.3°
Third rocker	50°–60°	55.9°

Table 3. Comparison between angles reported in[37,46,47] and angles obtained by the healthy condition.

in the second rocker is slightly above in comparison with the expected values, due to limitations of the model associated with the stiffness caused by the mesh (Table 3). The eversion and inversion generated by the foot in healthy conditions have some degree differences in contrast with kinematic mean patterns (Fig. 6).

Representation of stance period of the gait cycle

The biomechanical representation of the foot during a gait cycle was carried out through four continuous simulation steps using the nonlinear solver in ABAQUS/CAE software V.6.14-1. The first simulation step involved modeling the first rocker. During this rocker phase, the foot moves from dorsiflexion to ground contact (Fig. 7A). Once the first rocker is complete, the second simulation step begins, where boundary and loading conditions are adjusted to represent mid-stance. In this rocker phase, the foot is deformed by the load applied to
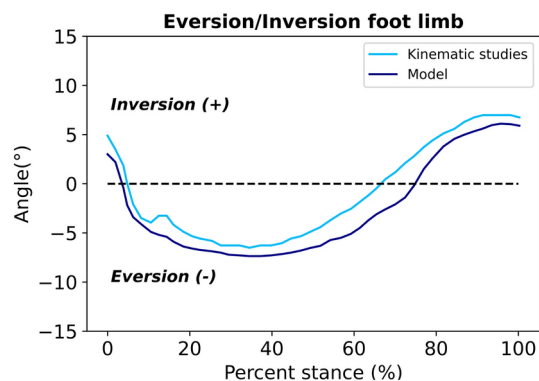
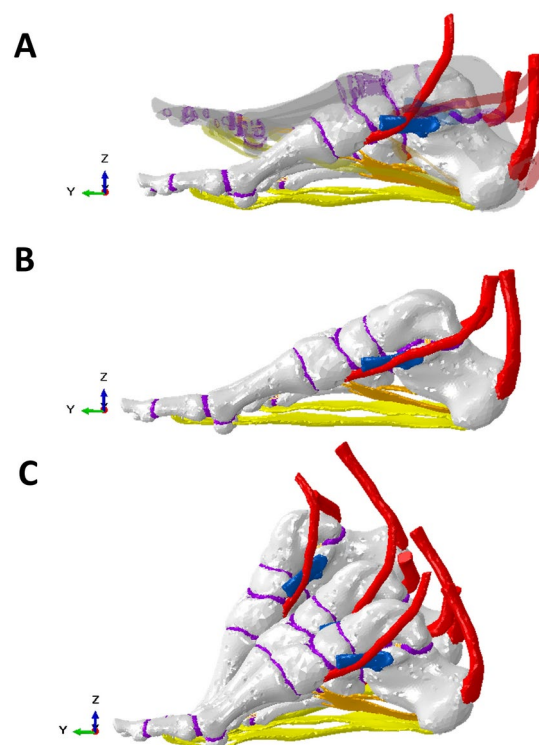**Fig. 6.** Eversion and inversion of the subtalar joint in the stance period.

Fig. 7. Model representation of foot biomechanics during the stance phase of the gait cycle.

the talus region (Fig. 7B). Following the completion of the second rocker, the third simulation step commences, with modified loading conditions to establish the scenario before the third rocker. Finally, the last simulation step represents the third rocker, where the calcaneus lifts off the ground, leading to plantarflexion of the foot (Fig. 7C).

Tissues stress analysis in the stance period

The PF and SL are the main tissues associated with conserving the plantar arch[33]. We measured the biomechanical stress generated in both tissues during gait analysis in healthy conditions. The *Smax* distribution in PF and SL during the stance period is shown in Fig. 8.

PF and SL findings were scaled their colors from 0 to 45.0 MPa and 0 to 25.0 MPa respectively. This change allows an adequate comparison. The *Smax* generated in SL is higher during the third rocker than the first and second rocker. Additionally, the stress in the PF is higher during the third rocker than the other rockers of the gait cycle. During heel rise, there is a notable stress concentration on the medial side of the PF. These results are consistent with expectations and demonstrate the applicability of this foot model.
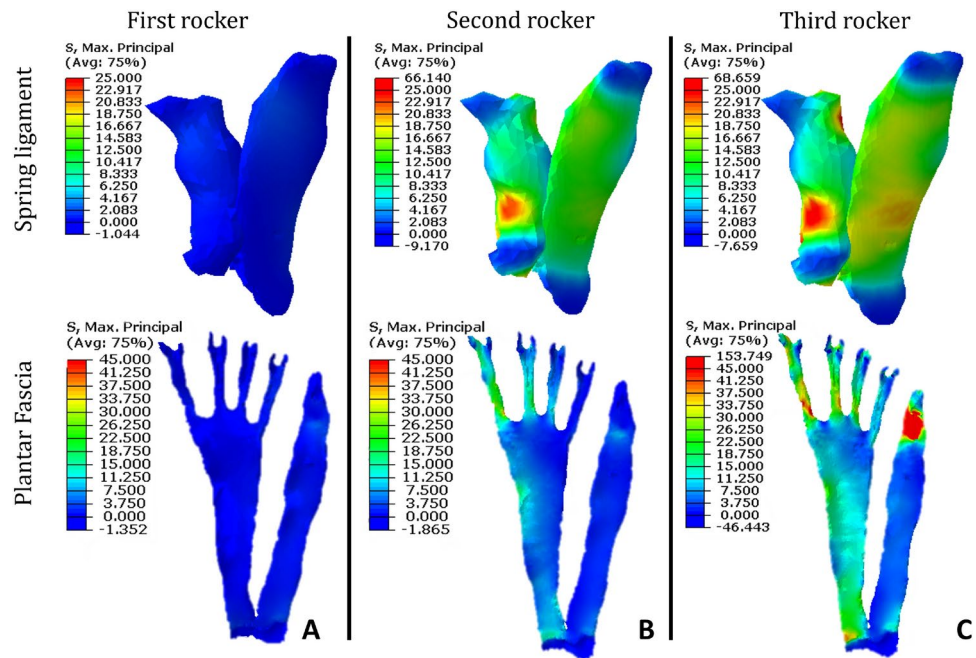
Fig. 8. *Smax* in PF and SL during stance period in healthy condition, (**A**) first rocker, (**B**) second rocker, and (**C**) third rocker. The scale color for the results of SL and PF were adjusted from 0 to 25.0 MPa and 0 to 45.0 MPa respectively.

Condition	Healthy	Spring ligament weakness	Fascia plantar weakness	Combined scenario
Healthy	− 8.29	–	–	–
Flatfoot	–	− 9.91	− 10.31	− 12.96
Partial subtalar arthrodesis	–	− 8.42	− 9.02	− 10.84
Triple arthrodesis	–	− 5.42	− 6.34	− 6.35

Table 4. Plantar arch fall in all the flatfoot and arthrodesis scenarios simulated in this study. Units of deformation are in millimeters.

Simulations for flatfoot and surgical scenarios

We measured the gradual deformation of the foot during healthy conditions, flatfoot, and by the application of the arthrodesis shown in Fig. 3. The deformation associated with the fall of the plantar arch was measured with nodes in the bottom region of the talus-navicular joint. In the healthy scenario (our reference), the plantar arch falls by 8.29 millimeters. However, under flatfoot conditions, the plantar arch drops even further than in the healthy scenario. In contrast, partial subtalar arthrodesis and triple arthrodesis result in a reduction of plantar arch collapse. A detailed summary of plantar arch fall can be found in Table 4.

Finally, we compare the changes of *Smax* over the PF and SL in all the investigated scenarios. The bar diagrams in Figs. 9 and 10 show a stress increase during the second rocker in PF and SL in flatfoot conditions and a decrease in stress during the second rocker in PF and SL when the foot has fusions in the hindfoot joints, especially in triple arthrodesis. In addition, the *Smax* in PF during the third rocker is higher on the lateral side in all considered situations, and it grows minimally on the medial area in flatfoot. The *Smax* decreases minimally in the medial and lateral sides of PF by partial subtalar arthrodesis (Fig. 11).

Discussion

The biomechanical studies currently reported in the literature for foot dynamics and tissue biomechanics are mainly obtained by external measurements because of the limitations of the cadaveric-model-based research. Over the last 30 years, cadaveric experiments have been used to study soft tissue behavior. However, these tests entail significant costs in acquiring the equipment used, and the physiological characteristics of the individuals studied do not allow an objective comparison between studies.

An alternative nowadays accepted by many clinicians and biomechanical researchers is the use of computational models. This investigation presents a computational human foot model that allows us to represent the foot biomechanics during the entire stance phase of the gait cycle, allowing the study of stress changes in soft tissues and foot deformity for some surgical scenarios. Our model has three key features. Firstly, most models reported in the literature simulate the stance period of gait as an independent static scenario[10–18]. This
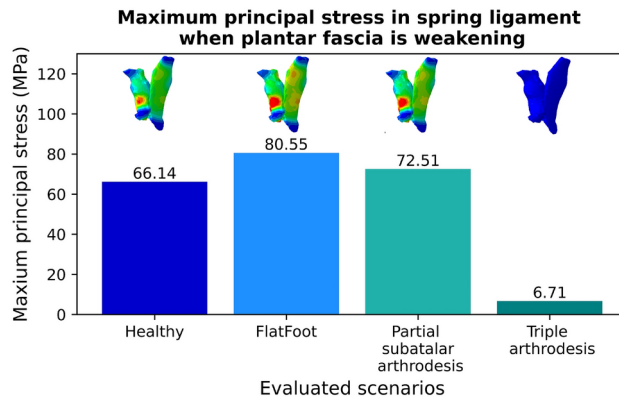
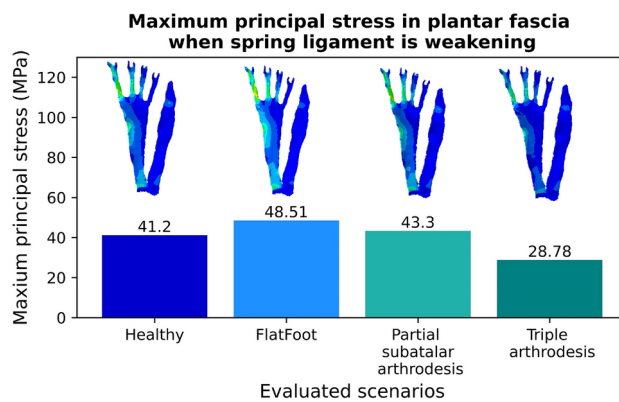**Fig. 9.** *Smax* in the medial side of the PF in all second rocker studied scenarios.

Fig. 10. *Smax* in the SL in all second rocker studied scenarios.
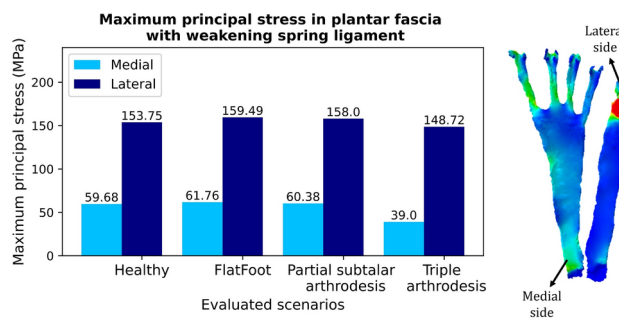

Fig. 11. *Smax* in PF in the third rocker.

assumption and simplification are not entirely accurate because the phases of the stance period constitute a continuous movement. Our model does not treat gait rockers as independent scenarios; instead, we simulate all stance phases continuously. Second, we employ three-dimensional elements representing soft tissues, such as tendons, ligaments, and the PF. This detail is highly significant because many models reported in the literature that simulates the stance period use bar elements to represent these tissues. While this allows for the representation of mechanical movement, it does not allow for the measurement of biomechanical stress changes caused in the tissues. Finally, the model includes the geometry and details of the main structures related to the arch support. The model considers trabecular bone, including all the foot joints with cartilage tissue, between other non-common considerations and could be considered a robust representation of the foot biomechanics.

The deformation results coincide with healthy clinical values[45], evaluated in terms of the IMCB and Kite's angle. Also, the metatarsophalangeal joint angle and eversion/inversion of the foot are in the range of kinematic angles. However, the metatarsophalangeal joint during the second rocker is not close to the kinematic angle reported in the literature. This happened because our computational model is a unique mesh in an unloaded

foot. This characteristic increases the stiffness of our model. Nonetheless, this issue does not affect the validation process and model results. Based on model validation the results and kinematic comparison, we can conclude that the model produces a good representation of foot biomechanics.

The results about *Smax* in the PF suggest that this tissue plays an active role in both the second and the third rocker. Specifically, higher stress is observed on the medial than lateral side during the second rocker. However, in the last phase of the gait cycle, the stress distribution exhibits a contrasting behavior compared to the second rocker. According to the study conducted by Ward et al.[48], the impulse of the PF during the gait cycle in the medial and lateral sides is not considerable in the heel strike (0–10% GC). In mid-stance (10–30% GC), there is a higher force in the medial zone compared to the lateral zone. Finally, in terminal stance (30–50% GC) to pre-swing (50–60% GC), the lateral side shows high-stress values until approximately 55% of GC, after which stress decreases dramatically. Simultaneously, the medial side experiences a moderate increase in impulse until nearly 58% of GC, after which the impulse decreases[48]. Our results showed similar behavior for the first and second rockers (Fig. 8). The findings for the third rocker differ because the boundary conditions used for the second to third rocker do not change as occurs in in-vivo gait situations. At the beginning of the third rocker, all the toes are in contact with the ground. However, as the foot starts to lift off the floor, some toes lose contact, indicating the need to modify the initially chosen boundary condition. Nevertheless, the strategy we used to simulate the model does not consider changes in boundary conditions during the simulation process, mainly because of software limitations. This limitation of the model should be considered when analyzing stress changes in this tissue across the different simulated scenarios.

The PF plays a crucial role in maintaining and supporting the longitudinal arch of the foot[29,49,50]. Additionally, some authors[51–53] have shown that in mid-stance, the primary load on the forefoot is supported in the first three metatarsals. The results in Fig. 8B show that stress distribution is located in the medial area of PF. These findings can be related to the function of PF in the maintenance of the plantar arch. Furthermore, the stress distribution is concentrated in the first two metatarsals, as reported in kinetic studies. Some studies[49,54] indicated that as the foot moves from mid-stance to pre-swing, the toes undergo dorsiflexion, leading to the tightening of the PF through its connections to the toes via the plantar plate. Our results in the third rocker (Fig. 8C) show a stress increment in the insertion of PF in the metatarsals. Also, during the third rocker, the PF completely tightens. Consequently, it increases the stress along the medial zone.

As well as the PF, the SL plays a crucial role in maintaining and supporting the longitudinal arch of the foot, mainly avoiding pronation in the second rocker[29,50,55]. The results of the *Smax* in the SL (Fig. 8B,C) suggest that this tissue has active participation during the second and third rockers. These findings were expected due to the deformation of the plantar arch during these stance phases. The plantar arch deformation leads to an elongation of the SL, which consequently increases *Smax* in SL. Therefore, the SL must participate as a stabilizer of the plantar arch. In contrast, in the first rocker (Fig. 8A) there is no relevant deformation of the plantar arch. Thus, it makes sense that the *Smax* in the SL during the first rocker is lower than other rockers, as our results suggest.

The plantar arch experienced a 20% decrease when the SL reduced its mechanical properties and a 24% reduction when the PF diminished its mechanical properties. When PF and SL had a reduction in their mechanical properties the plantar arch fall increased by about 56%. Therefore, these results confirm the assumption that the PF is one of the most important arch-supporter tissues[13,29]. Simulations performed of the arthrodesis scenarios show that, as was expected, this procedure helps to maintain the arch structure and reduce the fall of the plantar arch, especially triple arthrodesis. In those scenarios, we only focused our analysis on the second and third rockers because these rockers present the main stress changes in PF and SL. In flatfoot conditions during the second rocker, the stress in the SL increases by about 21.7% (Fig. 9), and the stress in PF increases by 17.7 % (Fig. 10). During the third rocker, our results show that the stress increases more in the lateral zone of the PF than in the medial region (Fig. 11), but these values could be altered by the fixed nodes on the lateral metatarsals required for the model.

In the course of the second rocker, the stability of the plantar arch depends on PF and SL. According to the results, if one of them fails, the plantar arch falls, and the other passive stabilizer assumes more charge and tries to avoid the total fall of the arch. Although there are some active stabilizers of the plantar arch, tendons are not enough to maintain it. The second rocker results agree with some validated computational model studies[13,33]. In flatfoot, the hindfoot exhibits greater pronation and adduction compared to healthy conditions[56]. Consequently, the increase in *Smax* in the medial area of the PF during the third rocker may be associated with the increased load resulting from these kinematic changes in the foot (Fig. 11).

Experimental researchers and case reports in the clinical literature regarding arthrodesis as a treatment for flatfoot commonly indicate favorable outcomes. The surgical techniques employed in these cases generally result in significant pain reduction and correction of foot structure. The results of surgical scenarios show that partial subtalar arthrodesis and triple arthrodesis reduce stress in the SL by 10% and more than 80%, respectively (Fig. 9). Similarly, partial subtalar arthrodesis and triple arthrodesis decrease PF stress by approximately 11% and 40.6%, respectively (Fig. 10). Additionally, partial subtalar arthrodesis slightly reduces stress in the PF during the third rocker. The reduction of stress on the PF and SL through arthrodesis is directly related to joint fusion, as it restricts and decreases foot deformation, as shown in Table 4. The results of this study suggest that arthrodesis is a good option for successfully correcting foot structure deformity and reducing stress on PF and SL. However, further research is needed to investigate the effects of bone joint fusions during the second and third rockers to determine the most appropriate treatment option.

We consider that the limitations of our model can be categorized into two main issues. The first point involves the exclusion of the plantar pad and the absence of the dorsiflexor and additional plantar flexor muscles of the foot. However, including the plantar pad does not modify the main results obtained but increases the computational cost of the model considerably. Dorsiflexor muscles play a role during the swing phase of the gait cycle, but their contribution during the heel strike and the loading response phase is relatively low[37,47]. The second issue relates

to boundary and load conditions. Although we have justified this critical aspect of the computational model based on existing literature, it does not entirely capture the complexities of real-life scenarios. We encountered convergence problems when simulating the third phase using only fixed nodes in the first, second, and third distal phalanges (as some toes lose contact with the floor during this phase). The cartilage material was unable to accommodate significant deformation. As a result, we opted to use fixed nodes across all distal phalanges of the toes. However, this adjustment in boundary conditions has a drawback, as the fixed nodes in the fifth distal phalange contribute to an increase in the $Smax$ on the lateral side of the PF. Additionally, the mechanical properties assigned to foot tissues are based on population averages. This assumption is not inaccurate for simulating foot biomechanics. The goal of this strategy is often to analyze variables such as von Mises stress, and maximum or minimum principal stress in tissues or orthopedic devices. For researchers aiming to enhance the precision of biomechanical stress analysis, incorporating statistical models that account for variations in mechanical properties of foot tissues across a range of simulations could improve the applicability of the model results in the clinical decision process.

Conclusion

The proposed computational model can represent the biomechanics of the foot during the entire stance phase of the gait cycle. The results of the PF and SL allow for the understanding and study of the biomechanics of these tissues during the first to the third rocker. Our findings show that PF and SL have different roles during the stance phase. The stress distribution in these passive stabilizers of plantar arch fits with the theory of their active role during mid-stance and pre-swing. Finally, the use of computational models can be considered to represent and analyze different scenarios of flatfoot and arthrodesis. This study offers an option for clinical research for quantifying tissue strain, expanding the tools available for analyzing foot biomechanics.

Data availability

The models and data generated during and/or analyzed during the current study are available from the authors upon reasonable request to the corresponding author.

References

1. Boulton, A. J. et al. Dynamic foot pressure and other studies as diagnostic and management aids in diabetic neuropathy. *Diabetes Care* **6**, 26–33. https://doi.org/10.2337/diacare.6.1.26 (1983).
2. Cavanagh, P., Ulbrecht, J. & Caputo, G. Biomechanical aspects of diabetic foot disease: Aetiology, treatment, and prevention. *Diabet. Med.* **13**, S17–S22. https://doi.org/10.1002/dme.1996.13.s1.17 (1996).
3. Alexander, I. J., Chao, E. Y. & Johnson, K. A. The assessment of dynamic foot-to-ground contact forces and plantar pressure distribution: A review of the evolution of current techniques and clinical applications. *Foot Ankle* **11**, 152–167. https://doi.org/10.1177/107110079001100306 (1990).
4. Balmaseda, M. Jr. et al. Ground reaction forces, center of pressure, and duration of stance with and without an ankle–foot orthosis. *Arch. Phys. Med. Rehabil.* **69**, 1009–1012 (1988).
5. Brown, M., Rudicel, S. & Esquenazi, A. Measurement of dynamic pressures at the shoe–foot interface during normal walking with various foot orthoses using the fscan system. *Foot Ankle Int.* **17**, 152–156. https://doi.org/10.1177/107110079601700306 (1996).
6. Lundeen, S., Lundquist, K., Cornwall, M. W. & McPoil, T. G. Plantar pressures during level walking compared with other ambulatory activities. *Foot Ankle Int.* **15**, 324–328. https://doi.org/10.1177/107110079401500607 (1994).
7. Rosenbaum, D., Bauer, G., Augat, P. & Claes, L. Calcaneal fractures cause a lateral load shift in chopart joint contact stress and plantar pressure pattern in vitro. *J. Biomech.* **29**, 1435–1443. https://doi.org/10.1016/0021-9290(96)84539-8 (1996).
8. Soames, R. Foot pressure patterns during gait. *J. Biomed. Eng.* **7**, 120–126. https://doi.org/10.1016/0141-5425(85)90040-8 (1985).
9. Wang, Y., Wong, D.W.-C. & Zhang, M. Computational models of the foot and ankle for pathomechanics and clinical applications: A review. *Ann. Biomed. Eng.* **44**, 213–221. https://doi.org/10.1007/s10439-015-1359-7 (2016).
10. Akrami, M. et al. Subject-specific finite element modelling of the human foot complex during walking: Sensitivity analysis of material properties, boundary and loading conditions. *Biomech. Model. Mechanobiol.* **17**, 559–576. https://doi.org/10.1007/s10237-017-0978-3 (2018).
11. Cheung, J.T.-M., Zhang, M., Leung, A.K.-L. & Fan, Y.-B. Three-dimensional finite element analysis of the foot during standing-a material sensitivity study. *J. Biomech.* **38**, 1045–1054. https://doi.org/10.1016/j.jbiomech.2004.05.035 (2005).
12. Chen, W.-P., Tang, F.-T. & Ju, C.-W. Stress distribution of the foot during mid-stance to push-off in barefoot gait: A 3-d finite element analysis. *Clin. Biomech.* **16**, 614–620 (2001).
13. Cifuentes-De la Portilla, C., Larrainzar-Garijo, R. & Bayod, J. Biomechanical stress analysis of the main soft tissues associated with the development of adult acquired flatfoot deformity. *Clin. Biomech.* **61**, 163–171 (2019).
14. Gefen, A., Megido-Ravid, M., Itzchak, Y. & Arcan, M. Biomechanical analysis of the three-dimensional foot structure during gait: A basic tool for clinical applications. *J. Biomech. Eng.* **122**, 630–639. https://doi.org/10.1115/1.1318904 (2000).
15. Mo, F., Li, Y., Li, J., Zhou, S. & Yang, Z. A three-dimensional finite element foot-ankle model and its personalisation methods analysis. *Int. J. Mech. Sci.* **219**, 107108 (2022).
16. Morales-Orcajo, E., Bayod, J., Becerro-de Bengoa-Vallejo, R., Losa-Iglesias, M. & Doblare, M. Influence of first proximal phalanx geometry on hallux valgus deformity: A finite element analysis. *Med. Biol. Eng. Comput.* **53**, 645–653 (2015).
17. Qian, Z., Ren, L., Ding, Y., Hutchinson, J. R. & Ren, L. A dynamic finite element analysis of human foot complex in the sagittal plane during level walking. *PLoS ONE* **8**, e79424. https://doi.org/10.1371/journal.pone.0079424 (2013).
18. Wang, Y., Li, Z., Wong, D.W.-C., Cheng, C.-K. & Zhang, M. Finite element analysis of biomechanical effects of total ankle arthroplasty on the foot. *J. Orthop. Transl.* **12**, 55–65. https://doi.org/10.1016/j.jot.2017.12.003 (2018).
19. Wang, Y., Wong, D.W.-C., Tan, Q., Li, Z. & Zhang, M. Total ankle arthroplasty and ankle arthrodesis affect the biomechanics of the inner foot differently. *Sci. Rep.* **9**, 13334 (2019).
20. Chen, T.L.-W. et al. Dynamic finite element analyses to compare the influences of customised total talar replacement and total ankle arthroplasty on foot biomechanics during gait. *J. Orthop. Trans.* **38**, 32–43. https://doi.org/10.1016/j.jot.2022.07.013 (2023).
21. Cifuentes-De la Portilla, C., Larrainzar-Garijo, R. & Bayod, J. Analysis of biomechanical stresses caused by hindfoot joint arthrodesis in the treatment of adult acquired flatfoot deformity: A finite element study. *Foot Ankle Surg.* **26**, 412–420 (2020).

22. Singh, G., Gupta, S. & Chanda, A. Biomechanical modelling of diabetic foot ulcers: A computational study. *J. Biomech.* **127**, 110699. https://doi.org/10.1016/j.jbiomech.2021.110699 (2021).
23. Jastifer, J. R. & Gustafson, P. A. Three-dimensional printing and surgical simulation for preoperative planning of deformity correction in foot and ankle surgery. *J. Foot Ankle Surg.* **56**, 191–195. https://doi.org/10.1053/j.jfas.2016.01.052 (2017).
24. Cifuentes-De la Portilla, C., Pasapula, C., Gutiérrez-Narvarte, B., Larrainzar-Garijo, R. & Bayod, J. Peroneus longus overload caused by soft tissue deficiencies associated with early adult acquired flatfoot: A finite element analysis. *Clin. Biomech.* **86**, 105383 (2021).
25. Lhoste-Trouilloud, A. The tibialis posterior tendon. *J. Ultrasound* **15**, 2–6. https://doi.org/10.1016/j.jus.2012.02.001 (2012).
26. Olewnik, Ł. A proposal for a new classification for the tendon of insertion of tibialis posterior. *Clin. Anat.* **32**, 557–565. https://doi.org/10.1002/ca.23350 (2019).
27. Burkhart, T. A., Andrews, D. M. & Dunning, C. E. Finite element modeling mesh quality, energy balance and validation methods: A review with recommendations associated with the modeling of bone tissue. *J. Biomech.* **46**, 1477–1488. https://doi.org/10.1016/j.jbiomech.2013.03.022 (2013).
28. García-Aznar, J. M. *et al.* Load transfer mechanism for different metatarsal geometries: A finite element study. *Unizar* (2009).
29. Tao, K., Ji, W.-T., Wang, D.-M., Wang, C.-T. & Wang, X. Relative contributions of plantar fascia and ligaments on the arch static stability: A finite element study. *Biomed. Tech. (Berl)*[SPACE]https://doi.org/10.1515/bmt.2010.041 (2010).
30. Wright, D. & Rennels, D. A study of the elastic properties of plantar fascia. *JBJS* **46**, 482–492 (1964).
31. Mansour, J. M. Biomechanics of cartilage. *Kinesiology: The mechanics and pathomechanics of human movement* **2**, 66–79 (2003).
32. Wu, L. Nonlinear finite element analysis for musculoskeletal biomechanics of medial and lateral plantar longitudinal arch of virtual chinese human after plantar ligamentous structure failures. *Clin. Biomech.* **22**, 221–229. https://doi.org/10.1016/j.clinbiomech.2006.09.009 (2007).
33. Cifuentes-De la Portilla, C., Larrainzar-Garijo, R. & Bayod, J. Analysis of the main passive soft tissues associated with adult acquired flatfoot deformity development: A computational modeling approach. *J. Biomech.* **84**, 183–190 (2019).
34. Fenton, R. M. Race walking ground reaction forces. In *ISBS-Conference Proceedings Archive* (1984).
35. Winiarski, S. & Rutkowska-Kucharska, A. Estimated ground reaction force in normal and pathological gait. *Acta Bioeng. Biomech.* **11** (2009).
36. Calhoun, J. H., Li, F., Ledbetter, B. R. & Viegas, S. F. A comprehensive study of pressure distribution in the ankle joint with inversion and eversion. *Foot Ankle Int.* **15**, 125–133. https://doi.org/10.1177/107110079401500307 (1994).
37. Jacquelin Perry, M. Ankle foot complex. In incorporated, S. (ed.) *Gait Analysis: Normal and Pathological Function*, 51–88 (1992).
38. Kirane, Y., Michelson, J. & Sharkey, N. A. Evidence of isometric function of the flexor hallucis longus muscle in normal gait. *J. Biomech.* **41**, 1919–1928. https://doi.org/10.1016/j.jbiomech.2008.03.040 (2008).
39. Arangio, G. A. & Salathe, E. P. A biomechanical analysis of posterior tibial tendon dysfunction, medial displacement calcaneal osteotomy and flexor digitorum longus transfer in adult acquired flat foot. *Clin. Biomech.* **24**, 385–390. https://doi.org/10.1016/j.clinbiomech.2009.01.009 (2009).
40. Orcajo, E. M. Computational foot modeling for clinical assessment. *Universidade Federal de Minas Gerais* (2015).
41. Giddings, V. L., Beaupre, G. S., Whalen, R. T. & Carter, D. R. Calcaneal loading during walking and running. *Med. Sci. Sports Exerc.* **32**, 627–634. https://doi.org/10.1097/00005768-200003000-00012 (2000).
42. Bogey, R., Perry, J. & Gitter, A. An emg-to-force processing approach for determining ankle muscle forces during normal human gait. *IEEE Trans. Neural Syst. Rehabil. Eng.* **13**, 302–310. https://doi.org/10.1109/TNSRE.2005.851768 (2005).
43. Kaya, D. Ö. Architecture of tendon and ligament and their adaptation to pathological conditions. In *Comparative kinesiology of the human body*, 115–147, https://doi.org/10.1016/B978-0-12-812162-7.00009-6 (Elsevier, 2020).
44. Barrett, J. M. & Callaghan, J. P. A mechanistic damage model for ligaments. *J. Biomech.* **61**, 11–17. https://doi.org/10.1016/j.jbiomech.2017.06.039 (2017).
45. Larrosa, M. & Mas Moliné, S. Alteraciones de la bóveda plantar. *Revista Espanola de Reumatologia* **30**, 489–498 (2003).
46. Bojsen-Møller, F. & Lamoreux, L. Significance of free dorsiflexion of the toes in walking. *Acta Orthop. Scand.* **50**, 471–479. https://doi.org/10.3109/17453677908989792 (1979).
47. Brockett, C. L. & Chapman, G. J. Biomechanics of the ankle. *Orthopaedics Trauma* **30**, 232–238. https://doi.org/10.1016/j.mporth.2016.04.015 (2016).
48. Ward, E. D., Smith, K. M., Cocheba, J. R., Patterson, P. E. & Phillips, R. D. In vivo forces in the plantar fascia during the stance phase of gait: Sequential release of the plantar fascia. *J. Am. Podiatr. Med. Assoc.* **93**, 429–442. https://doi.org/10.7547/87507315-93-6-429 (2003).
49. Hedrick, M. R. The plantar aponeurosis. *Foot Ankle Int.* **17**, 646–649. https://doi.org/10.1177/107110079601701012 (1996).
50. Huang, C.-K., Kitaoka, H. B., An, K.-N. & Chao, E. Y. Biomechanical evaluation of longitudinal arch stability. *Foot Ankle* **14**, 353–357. https://doi.org/10.1177/107110079301400609 (1993).
51. Hughes, J., Clark, P., Linge, K. & Klenerman, L. A comparison of two studies of the pressure distribution under the feet of normal subjects using different equipment. *Foot Ankle* **14**, 514–519. https://doi.org/10.1177/107110079301400905 (1993).
52. Rodgers, M. M. Dynamic foot biomechanics. *J. Orthop. Sports Phys. Ther.* **21**, 306–316, https://doi.org/10.2519/jospt.1995.21.6.306 (1995).
53. Prutchi, D. & Arcan, M. Dynamic contact stress analysis using a compliant sensor array. *Measurement* **11**, 197–210. https://doi.org/10.1016/0263-2241(93)90039-K (1993).
54. Hicks, J. The mechanics of the foot: Ii. The plantar aponeurosis and the arch. *J. Anat.* **88**, 25 (1954).
55. Steginsky, B. & Vora, A. What to do with the spring ligament. *Foot Ankle Clin.* **22**, 515–527. https://doi.org/10.1016/j.fcl.2017.04.005 (2017).
56. Shin, H. S. et al. Flatfoot deformity affected the kinematics of the foot and ankle in proportion to the severity of deformity. *Gait & Posture* **72**, 123–128. https://doi.org/10.1016/j.gaitpost.2019.06.002 (2019).

Acknowledgements

Author contributions

Conceptualization, methodology, visualization, writing—original draft preparation, formal analysis, and investigation: N.Y.M. and C.J.C.; Project administration and writing—review and editing: N.Y.M., J.B., and C.J.C.; Supervision: J.B. and C.J.C. All authors have read and agreed to the published version of the manuscript.

Declarations

Competing interests
The authors declare no competing interests.

Additional information
Correspondence and requests for materials should be addressed to C.C.-D.

Reprints and permissions information is available at www.nature.com/reprints.

Publisher's note Springer Nature remains neutral with regard to jurisdictional claims in published maps and institutional affiliations.